

Microstructure evolution in magnetorheological suspensions governed by Mason numberSonia Melle,^{1,2} Oscar G. Calderón,³ Miguel A. Rubio,² and Gerald G. Fuller¹¹*Department of Chemical Engineering, Stanford University, Stanford, California 94305-5025, USA*²*Departamento de Física Fundamental, UNED, Senda del Rey 9, Madrid 28040, Spain*³*Departamento de Óptica, Universidad Complutense de Madrid, Ciudad Universitaria, Madrid 28040, Spain*

(Received 19 February 2003; published 20 October 2003)

The spatiotemporal evolution of field-induced structures in very dilute polarizable colloidal suspensions subject to rotating magnetic fields has been experimentally studied using video microscopy. We found that there is a crossover Mason number (ratio of viscous to magnetic forces) above which the rotation of the field prevents the particle aggregation to form chains. Therefore, at these high Mason numbers, more isotropic clusters and isolated particles appear. The same behavior was also found in recent scattering dichroism experiments developed in more concentrated suspensions, which seems to indicate that the dynamics does not depend on the volume fraction. Scattering dichroism experiments have been used to study the role played by the volume fraction in suspensions with low concentration. As expected, we found that the crossover Mason number does not depend on the volume fraction. Brownian particle dynamics simulations are also reported, showing good agreement with the experiments.

DOI: 10.1103/PhysRevE.68.041503

PACS number(s): 83.80.Gv, 75.50.Mm, 82.70.Dd, 45.50.-j

I. INTRODUCTION

Magnetorheological (MR) suspensions are essentially suspensions of magnetizable particles immersed in a nonmagnetic fluid. These complex fluids show a unique ability to undergo rapid, nearly completely reversible, significant changes in their mechanical and optical properties upon application of an external magnetic field [1]. The physical origin of this behavior is that, under the action of an external field, the particles acquire a magnetic dipole moment, which, due to dipolar interaction, induce particle aggregation to form chainlike structures aligned with the field. This change in suspension microstructure is accompanied by significant changes in flow behavior and optical properties because these structures restrict the motion of the fluid, thereby increasing the viscosity of the suspension, and induce optical anisotropy. The potential applicability of such fluids has stimulated considerable research activity in developing devices such as controllable shock absorbers, electromagnetic clutches and brakes, control valves, and artificial joints [2,3], as well as other microfluidic devices which involve lower concentrate magnetorheological suspensions especially for biomedical applications [4,5]. On the other hand, and from a more fundamental point of view, the relationship between microscopic structure and mechanical and optical properties of these systems has excited considerable interest in the last decade [6–8].

Most of the studies to date have focused on the optical response of MR suspensions to unidirectional magnetic fields [8–13]. However, in the past years their dynamical response to rotating magnetic fields has been a new research area of interest. Indeed, the rotating field configuration closely resembles the simple shear configuration appearing in most of the practical applications of MR fluids. Moreover, the rotating field experiments have a much simpler laboratory implementation than a simple shear experiment, which requires precise mechanical motion. Thus, pioneering experimental studies were reported on magnetic holes (nonmagnetic mi-

crosheres in a ferrofluid) [14,15], magnetic microdroplets [16], and MR suspensions [17–20] subject to rotating magnetic fields. These systems show a rich dynamics depending on the value of the rotating field frequency. The response of a pair of magnetic particles immersed within a fluid was first experimentally reported by Kashevsky and Novikova [17]. Later on, some theoretical works described the different rotation modes of systems formed by few magnetic particles under rotating fields [18]. At very high rotating field frequencies, these modes became extremely complicated and chaotic states were found. Colloidal suspensions subjected to high-frequency rotating fields have been recently studied [21–25]. They reported aggregation of particles into two-dimensional sheetlike structures aligned in the field plane.

The dynamics of semidilute MR fluids (volume fraction $\phi \sim 0.02$) under rotating magnetic fields has been recently studied using scattering dichroism [26,27]. In these suspensions, dichroism is caused by the polarization-dependent scattering from oriented aggregates [28] and, provided that there is no lateral aggregation, the scattering dichroism is proportional to the total number of aggregated particles, N_a [27]. We found that the field-induced chains rotate synchronously with the field but lag behind by a frequency-dependent phase angle. Qualitatively similar results were obtained in Ref. [29] in a system of magnetic microdroplets. Furthermore, a more relevant result arises from Ref. [27]: the Mason number, Ma (ratio of viscous to magnetic forces), governs the chain dynamics under rotating fields. This dimensionless parameter has been defined with different proportionality factors in the literature [24,30,31]. Here we use the following definition:

$$Ma = \frac{12^2 \eta \omega}{\mu_0 \mu_s M^2}, \quad (1.1)$$

where η is the solvent viscosity, ω is the rotating field frequency, μ_0 and μ_s are the vacuum and solvent magnetic

permeability, respectively, and \vec{M} is the particle magnetization. Here the proportionality factor has been chosen to be in agreement with the dimensionless frequency obtained from the simulations analysis (Sec. III). A change in behavior of the dichroism and the phase lag was found above a crossover Mason number $\text{Ma}_c \sim 1$, where the viscous forces dominate and inhibit the aggregation process.

In this paper, we report on an experimental video microscopy study of the aggregation of magnetizable particles and the subsequent chain orientation dynamics under rotating magnetic fields. This technique allows us to directly visualize the dynamics of very dilute suspensions ($\phi \sim 10^{-4}$). Note that the scattering dichroism technique will not be useful to study very dilute suspensions $\phi < 0.001$ due to the small dichroism signal obtained. We used different rotating frequencies which correspond to Mason numbers below and above 1, i.e., around the value where both magnetic and hydrodynamic interactions are comparable. This range of Mason numbers is similar to the one used in our previous scattering dichroism experiments in more concentrated suspensions [26,27]. We find that the average size of the aggregates decreases with Ma . Furthermore, we find a transition in the total number of aggregated particles at a crossover Mason number close to $\text{Ma}_c \sim 1$, in agreement with our previous work. Therefore, this result seems to indicate that the dynamics does not depend on the volume fraction, at least between $\phi \sim 10^{-4}$ and $\phi \sim 0.02$. In order to verify this result, we analyze the role played by the volume fraction in the dynamics using scattering dichroism experiments. As expected, we found that the crossover Mason number does not depend on the volume fraction, which points out the generality of this behavior. Our experimental findings have been corroborated through Brownian particle dynamics simulations of “hard” spheres with induced dipolar interactions and Stokes friction against the solvent. The simulations are in agreement with the experiments. We also developed numerical simulations to analyze the thermal effect on the dynamics.

II. EXPERIMENTS

Two experimental setups were used to study the dynamics governing MR suspensions subject to rotating magnetic fields. First, we performed video microscopy experiments on very dilute suspensions ($\phi \sim 10^{-4}$) to directly visualize their dynamics. Second, to study the role played by the volume fraction, scattering dichroism technique was needed since it allows the use of suspensions with moderate concentration. So we performed scattering dichroism experiments on suspensions with different volume fractions ranging from $\phi = 0.001$ to $\phi = 0.02$.

A. Experimental materials and procedure

1. Magnetic suspensions

To prepare our samples we used an aqueous suspension M1-070/60 of super-paramagnetic microspheres supplied by Estapor with a solid content of 10% in weight. The particles in the suspension contain magnetite crystals (Fe_3O_4) of small diameter (1–20 nm) dispersed in a polymeric matrix.

TABLE I. Properties of the magnetizable microspheres.

Particle properties	M1–070/60
Mean diameter (μm)	1.24
Magnetic content	61%
Saturation field (emu/g)	51.9
Surface group content ($\mu\text{eq/g}$)	117

The surface of the microspheres contains carboxylic acid ($-\text{COOH}$) groups with an added surfactant coating layer of sodium dodecyl sulfate (SDS) to stabilize the dispersions. The particles’ physical properties are detailed in Table I. We have characterized the average magnetic properties of the particles by measuring their magnetization curve using a vibrating sample magnetometer (VMS-Lakeshore 7300). We observed that under sufficiently low magnetic fields these particles exhibit super-paramagnetic behavior with virtually no hysteresis or magnetic remanence. Due to their small average diameter and density ($\rho_p \sim 1.3$ g/ml) the sedimentation time is long enough to neglect gravitational effects. The sedimentation velocity was estimated according to the Stokes’ law to be $v_s \sim 0.06$ $\mu\text{m/s}$.

For video microscopy experiments we diluted the suspension M1-070/60 with Milli-Q ultrapure water with the same SDS concentration as the original suspension in order to avoid particle aggregation. The volume fraction achieved is $\phi \sim 10^{-4}$. To analyze the volume fraction effect through scattering dichroism experiments, we prepared suspensions with 50% glycerol and different volume fractions ranging from $\phi \sim 0.02$ to $\phi \sim 10^{-3}$.

2. Magnetic field generation and sample cell

The video microscopy experiments requires optical transparency, so the fluid sample was sandwiched between two circular quartz windows with inner diameter 6.5 mm. These windows were held in place by a delrin attachment designed to prevent evaporation of the solvent and separated by an annular delrin spacer $e = 100$ μm thick along the light path (axis Z). The video microscopy images were taken at an area in the cell less than 1 mm in the vicinity of the center. The sample is placed at the center of two orthogonal pairs of coils that generate a rotating magnetic field in the plane of the images (XY). The rotating magnetic field was achieved by applying sinusoidal electric signals to the two orthogonal pairs of coils by means of two Kepco BOP20-10M power amplifiers, driven by two HP-FG3325A function generators referenced to one another at a phase difference of 90° . The function generators allowed for control of both the amplitude and the frequency of the rotating magnetic field. These coils are housed in a temperature controlled aluminum cylinder to prevent heating effects. All experiments were performed at a temperature of $T = 282 \pm 1$ K on the sample. The coil’s relative positions and their dimensions were optimized to obtain the smallest possible spatial variation of the field over the sample (smaller than 3% across the whole sample). This minimizes possible local changes of concentration due to

TABLE II. Summary of the experimental conditions.

Experimental conditions	Video microscopy	Scattering dichroism
Glycerol content	0%	50%
Volume fraction	$\phi=0.0001$	$\phi=0.02-0.001$
Field strength (kA/m)	$H=1.55$	$H=3.1$
Field frequency (Hz)	$f=0.001-1$	$f=0.001-15$
Figures	Figs. 1-3	Figs. 4 and 5

migration of the magnetic particles under the effect of field gradients. In Table II are summarized the experimental conditions for each experiment.

3. Video microscopy setup and procedure

We illuminated the top side of the sample from the direction perpendicular to the field plane using a white light source (*American Optical II-80*). To amplify the image we used a (*Navitar 12X*) zoom system composed of a 2X adapter that attaches the zoom to a charge-coupled-device (CCD) video camera (*Sanyo VDC-3825*), a 12X zoom, and a 2X attachment that joins the zoom to a 10X microscope objective placed close to the bottom side of the sample. This group of lenses has the advantage of combining large zoom range, high resolution, and long working distance (33 mm). This zoom system has the capability of allowing the field of view to be altered by changing the image resolution. The resolution could be varied between 0.34 and 4.2 $\mu\text{m}/\text{pixel}$ for fields of view between 170 and 2100 μm , respectively. The CCD camera is connected to a S-VHS VCR (*Panasonic AG 1975*) which records images at 30 frames/sec. We subsequently digitalized single frames of 640×480 pixels with 256 gray levels on a computer at fixed time intervals depending on the field rotational frequency. To analyze the images we used IGOR Pro image-processing software from *WaveMetrics, Inc.* The images had a dark background over which the particles appear as clear areas. In the image analysis the pixel area for each aggregate was calculated by applying a gray level threshold that was kept constant for a given experiment.

A typical experimental run would begin with an homogeneous sample and then we applied the rotating magnetic field for 365 sec. Although the zoom magnification was varied for each experiment to adapt the field of view, a resolution that allowed us to see individual particles was always used. Then, the temporal evolution of the total number of aggregated particles was determined. The average rotation angle of the chains was also computed by analyzing the Hough transform of the images [32,33].

4. Scattering dichroism setup and procedure

The optical train used to measure linear dichroism consists of a He-Ne laser, a polarizer (that sets the angle for the polarization), a photoelastic modulator (set at $\pi/4$ displacement with respect to the polarizer), and a quarter wave plate (set parallel to the polarizer). The laser beam goes through the sample cell and the transmitted light is detected by a photodiode. The signal from the photodiode is sent to a dc

amplifier to recover the dc component and two phase lock-in amplifiers (Priceton Applied Research, EG&G-128A) set at once and twice the photoelastic modulator frequency. The outputs of both lock-ins and the dc amplifier output are then digitized using a 16-bit resolution A/D data acquisition board (National Instruments, PCI-MIO-16xE-10). A full description of this experimental technique can be found in Refs. [26,34]. With this optical setup we can simultaneously measure the time evolution of the dichroism $\Delta n''(t) = n''_{\parallel} - n''_{\perp}$, i.e., the difference between the extinction of the incident light with polarization parallel and perpendicular to the long axis of the aggregates (being $n_{\parallel} = n'_{\parallel} - i n''_{\parallel}$ the refractive index in the direction parallel to the long axis of the aggregates). We can also measure the temporal evolution of the orientation angle of the aggregates θ'' , i.e., the average angle difference between the reference angle of the optical train and the long axis of the aggregates. By comparing θ'' with the temporal evolution of the magnetic field direction, given by ωt , we may define the phase lag between the field and the aggregates as $\alpha(t) = \omega t - \theta''(t)$.

The measurement procedure required, first, to set the values of frequency and amplitude of the magnetic field, second, to measure the time evolution of $\Delta n''(t)$ and $\theta''(t)$ until a steady state is reached, $\Delta n''_0$ and θ''_0 , and third, to wait the time necessary for the particles to break apart and to return to their initial state. Therefore, all measurements are independent, because there is no continuous sweep in either field frequency or amplitude.

B. Video microscopy results

In Fig. 1 video microscopy images show the temporal evolution of the structures induced by a magnetic field rotating clockwise with frequency $f=0.001$ Hz and amplitude $H=1.55$ kA/m ($\text{Ma}=0.0012$). When the field is first applied ($t=0$ s), a magnetic dipole is induced in each particle in the direction of the field. At this low volume fraction ($\phi \sim 10^{-4}$) the dipolar interaction induces particle aggregation into linear chains that follow the magnetic field direction. We have seen that the chains rotate synchronously with the field as was reported in Ref. [35]. The average chain length initially increases until it finally reaches a steady state [35]. Note that the aggregation kinetics under rotating magnetic fields is very different than the kinetics reported under unidirectional magnetic fields where power-law behavior governs the long-time aggregation regime [12,13]. Under rotating magnetic fields, the final size of the aggregates is roughly determined by the competition between the magnetic dipolar interaction and the hydrodynamic forces on the chains [36]. We observe that rotating chains undergo a process of dynamic chain growth and fragmentation that has a frequency twice that of the field frequency as was reported in Ref. [35].

We would like to emphasize that lateral aggregation of chains has not been observed at the low volume fractions reported in the video microscopy experiments as occur in unidirectional magnetic fields [9]. In the case of rotating fields, we have observed partial overlapping of chains at low rotational frequencies. This phenomenon is originated by a different mechanism than the lateral aggregation of chains

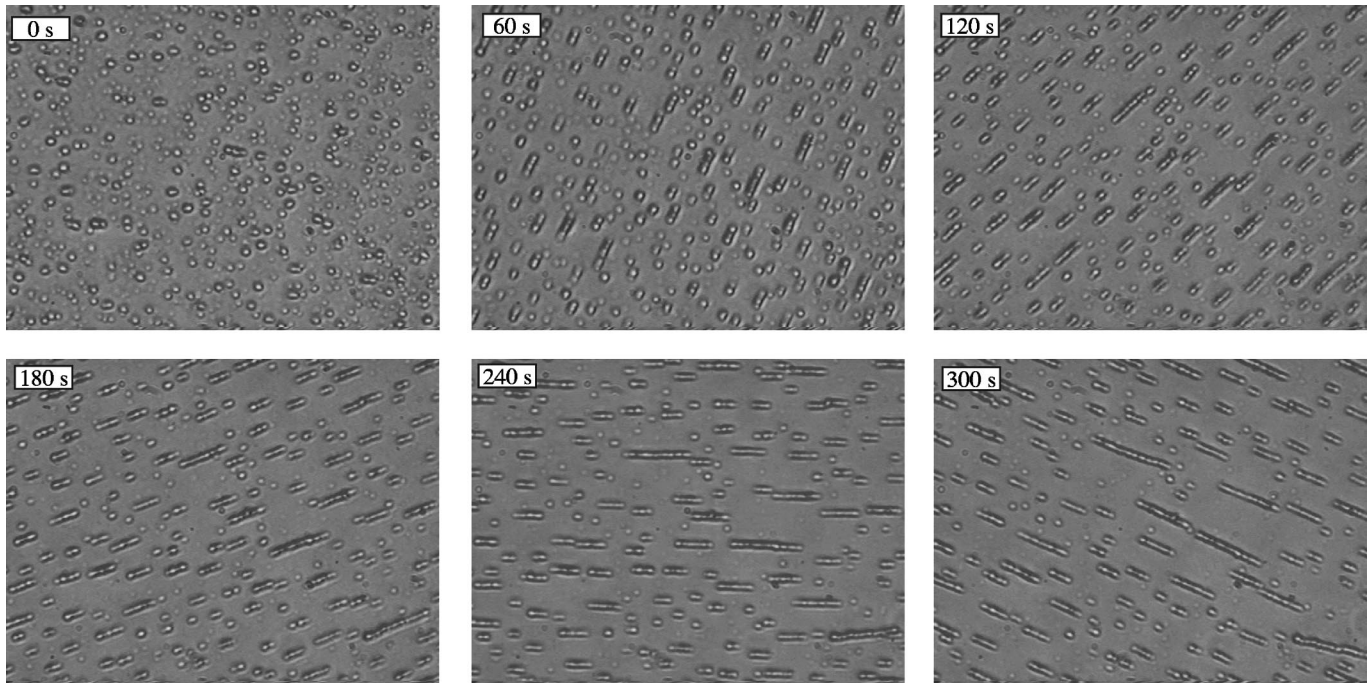


FIG. 1. Video microscopy images at different times showing the structures induced by a magnetic field rotating clockwise with frequency $f=0.001\text{Hz}$ and amplitude $H=1.55\text{kA/m}$. Field of view: $58\times 43\mu\text{m}^2$; suspensions with $\phi\sim 10^{-4}$.

under unidirectional fields since it is due to contact of close neighboring chains during their rotation when the distance between their centers is smaller than the average length of the chains. We observe that partial overlapping of chains always occurs in the plane perpendicular to the image since in this configuration the structure formed by two overlapping chains presents smaller inertia moment and is able to easily follow the field. Two dimensional sheets (several particles thick) aligned in the plane of the field were reported by Martin *et al.* [21,25,37] for high volume fraction suspensions under high-frequency rotating fields.

In the limit of low rotational frequencies, and for this low value of the magnetic field, aggregation and fragmentation processes are continuously observed between neighboring chains. Chains approach each other and, for a short time, they keep attached together by their ends and rotate as one. The phase lag of the longer formed chain respect to the field direction increases compared to the phase lag of the shorter chains. Hydrodynamic forces on the chains cause them to break up into smaller segments in order to remain oriented with the field (see Fig. 1), so finally the long chain breaks into shorter ones. The breakup process of a chain induced when a magnetic field of frequency $f=0.01\text{Hz}$ is applied can be qualitatively explained as follows (see Fig. 2). First, the chain deforms slightly from the straight configuration [Fig. 2(a)], later it develops a clearer S shape whose ends are aligned in the field direction [Fig. 2(b)]. Finally, the chain breaks up in two or more shorter structures [Fig. 2(c)] which can follow the field rotation more easily. Theoretical chain models developed for the case of electrorheological (ER) suspensions subject to a simple shear flow in the direction perpendicular to the field [38] and for MR suspensions subject to rotating fields [36] qualitatively account for the ob-

served S shape. Similar behavior has been observed also in magnetic microdroplets under rotating magnetic fields [29]. Thus, at long times, the average length shows strong temporal fluctuations which may be attributed to interchange of particles between chains in the fragmentation and aggregation process [35].

In Fig. 3 video microscopy images show the behavior of the structures induced for different rotational frequencies. All the images have been recorded after applying the field during $t=300\text{s}$. We can see that the length of the induced aggregates, L , decreases when increasing the frequency. The same behavior $L\propto\text{Ma}^{-1/2}$ is also obtained for a chain model in the case of rotating magnetic fields [35,36]. However, for $\text{Ma}\geq\text{Ma}_c\sim 1$, this low amplitude magnetic field is not strong enough for the structures to remain aligned in the field direction. Hence, at high frequencies ($f=1\text{Hz}$ in Fig. 3, which corresponds to $\text{Ma}=1.2$) even two particle chains may break apart, therefore increasing the number of isolated particles; moreover, other more isotropic structures appear, as for example disklike structures formed by 3–5 particles. Similar

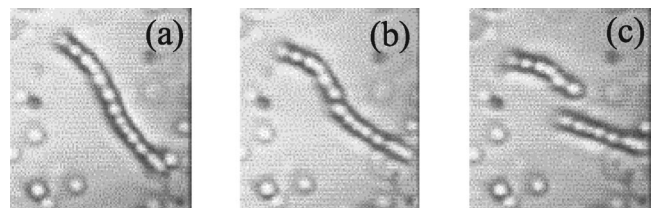


FIG. 2. Details of the S shape (reversed in this case) developed by one chain just before the breakup. The field rotates counterclockwise with frequency $f=0.01\text{Hz}$ ($\text{Ma}=0.012$). Field of view: $14.4\times 14.2\mu\text{m}^2$; suspensions with $\phi\sim 10^{-4}$.

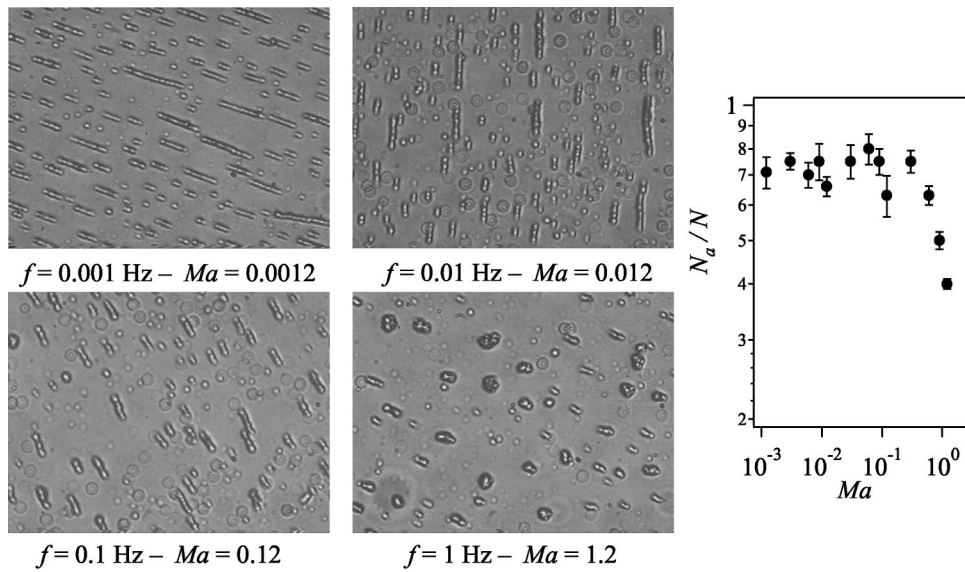


FIG. 3. (left) Video microscopy images at time=300 sec showing the structures induced in the suspension at different rotational frequencies ranging from $f = 0.001 \text{ Hz}$ ($Ma=0.0012$) to $f = 1 \text{ Hz}$ ($Ma=1.2$). Field of view: $58 \times 43 \mu\text{m}^2$; suspensions with $\phi \sim 10^{-4}$ (right). Variation of the normalized total number of aggregated particles with Ma .

structures were found for ER fluids subjected to high-frequency rotating fields [39]. Therefore the total number of aggregated particles should decrease when increasing Mason number. In Fig. 3 (on the right) we see the dependence of the normalized total number of aggregated particles with Mason number, which shows the expected behavior, in agreement with our previous work [27]. A deeper insight in the behavior of N_a (see Fig. 3) reveals that the crossover Mason number seems to be shifted to values lower than 1. We should say at this point that the criteria we followed to compute Ma_c is to consider the value at which a change in behavior is observed. Usually, this change is not abrupt but occurs in a range of values, therefore a precise determination of Ma_c cannot be made without some ambiguity. A possible responsible mechanism for the shift observed on Ma_c to smaller values is the formation of small structures displayed in the direction perpendicular to the image plane at high rotating frequencies (close to $Ma \approx 1$). From the image analysis, this fact leads to a decrease of the normalized total number of aggregated particles, and therefore it could explain the mentioned curve shift.

In summary, we have seen that the behavior of the very dilute MR suspensions is the same as found in our previous work on more concentrated suspensions, that is, there is a crossover Mason number ($Ma_c \sim 1$) above which the rotation of the field prevents the particle aggregation process into chains from taking place, and other more isotropic structures appear. This result seems to indicate that this scenario is basically independent of the volume fraction.

C. Scattering dichroism results

In Fig. 4 we plot the variation of the dichroism (left) and the phase lag (right) with rotational frequency for decreasing values of ϕ . We see, in agreement with our previous works for larger ϕ [26,27], that dichroism shows two distinct regions for frequencies below and above a crossover frequency f_c . Below this crossover frequency, the dichroism is essentially independent of frequency. However, once this frequency is surpassed, the dichroism strongly decreases with frequency following a power-law behavior with an exponent -1 . The phase lag also show two different responses de-

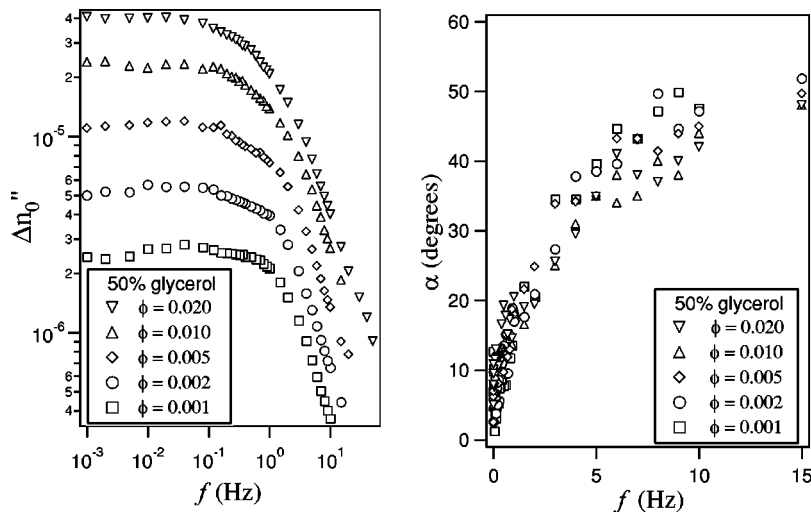


FIG. 4. Variation of the steady dichroism (left) and of the steady phase lag (right) with rotational frequency. Suspensions with 50% glycerol content, $0.001 < \phi < 0.02$; field amplitude $H = 3.1 \text{ kA/m}$.

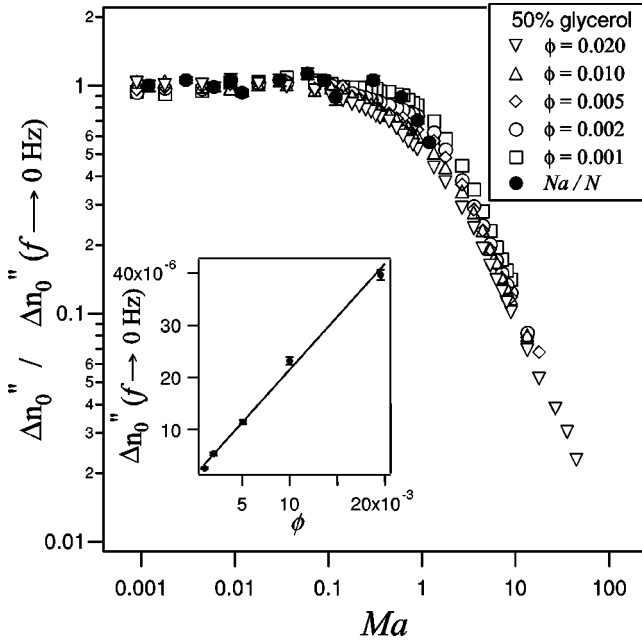


FIG. 5. Steady dichroism normalized with the dichroism at low frequencies vs Mason number (open symbols). Average dichroism at low frequencies vs the volume fraction (inset). Suspensions with 50% glycerol content, $0.001 < \phi < 0.02$; field amplitude $H = 3.1$ kA/m. For comparison, the normalized total number of aggregated particles corresponding to the video microscopy experiments has also been included (dots).

pending on the magnitude of frequency. At low frequencies (below f_c) the phase difference grows very quickly, while at high frequencies the increase of the phase lag is relatively slow. For frequencies larger than the crossover frequency, fewer and shorter chains survive, and so the contribution to the total dichroism and average phase lag is due to the few small chains that still remain. These small chains lag behind the magnetic field with larger phase angles since they are close to breaking apart.

As expected, the value of the dichroism at very low frequencies is different for different volume fractions since the number of particles in the measured area changes with the volume fraction. If we calculate the average value of the dichroism at low frequencies, where the dichroism remains constant, $\Delta n_0''(f \rightarrow 0)$, we observe that this value is proportional to the volume fraction (see inset in Fig. 5). This linear dependence of the volume fraction with the dichroism is due to the fact that for these low frequencies most of the particles are aggregated into chains.

In Fig. 5 we plot the dichroism normalized with the average dichroism measured at low frequencies, $[\Delta n_0'']/[\Delta n_0''(f \rightarrow 0)]$, versus Mason number. We can see a nice collapse of the curves for different volume fractions onto a master curve, and it is also apparent that the crossover Mason number does not change with the volume fraction. Therefore it is expected that at lower ϕ values the physical response of the system is similar. For comparison purposes we have also included in Fig. 5 the video microscopy results showed previously in Fig. 3. We see that both experiments roughly present the same behavior. Furthermore, a significant broadening of the

transition around the crossover Mason number as the volume fraction increases is observed, which could be observed at the left part of Fig. 4. At low volume fractions the rupture of the dimers leads to the abrupt change in dichroism behavior. However, at high volume fractions the mean distance between chains can be very small, so before the dimers break apart, they have a higher probability to join together with neighboring dimers forming more isotropic structures. Therefore, the collision of dimers around the crossover Mason number may lead to a broadening of the transition. Although it is not plotted here, a nice collapse of the curves corresponding to the phase lag is also found.

III. NUMERICAL SIMULATIONS AND DISCUSSION

A. Equations of motion

A complete algorithm to simulate MR fluids would include Brownian motion, multipolar magnetic interaction forces between the particles, local field corrections to the applied field, hydrodynamic friction forces (lubrication and long range), excluded-volume repulsive forces, and so on. However, our approach has been to consider only those contributions which we believe are essential to capture the physics of the problem. Therefore, in order to interpret the experimental results, we developed two-dimensional (2D) Brownian particle simulations of “hard” spheres with induced dipolar interactions and Stokes friction against the solvent. Similar approaches have been previously used [25,40–42]. We consider a monodisperse suspension of N spherical particles of diameter $2a$ suspended in a fluid of viscosity η and subjected to a rotating magnetic field of amplitude H and angular frequency ω . Taking into account that the aggregation takes place in the plane of the magnetic field rotation [17], we simplified our calculation by developing 2D simulations in this plane. Two fundamental length scales characterize the formation of chains. The first one is the so-called “thermomagnetic distance” R_1 , which is the distance at which the magnetic energy corresponding to the dipolar interaction between two particles aligned in the field direction and with parallel dipole moments equals the thermal fluctuation energy. This length scale turns out to be $R_1 = 2a\lambda^{1/3}$, where λ is a dimensionless parameter calculated as the ratio between magnetic and thermal energies,

$$\lambda \equiv \frac{W_m}{k_B T} = \frac{\mu_0 \mu_s m^2}{16\pi a^3 k_B T}, \quad (3.1)$$

where $m = (4\pi/3)a^3 M$ with M the particle magnetization, k_B is the Boltzmann constant, and T is the temperature. The physical meaning of R_1 is that particles that are separated by a distance larger than R_1 do not “feel” the magnetic interaction due to each other, because the energy of thermal fluctuations is larger than the dipolar interaction energy. The second length scale is the average initial interparticle distance, which can be estimated as $R_0 \sim 2a/\phi^{1/3}$ [13]. Actually, the values of λ that correspond to the experimental results reported here are $\lambda = 213$ for the video microscopy experiments with very dilute suspensions and $\lambda = 75$ for the scat-

tering dichroism experiments with more concentrated suspensions. In these experiments, since R_1 is typically $4 \leq R_1 \leq 7.5$, and R_0 is in the range $4 \leq R_0 \leq 20$, we will include the Brownian motion of the particles on the evolution of the structures. As a first approximation, we will neglect hydrodynamic interaction, and the only solvent effect that we will consider is the viscous force represented as a Stokes force acting on each particle. We can typically neglect the inertial term in the equation of motion because the viscous drag term dominates. Therefore, the equation of motion for the i particle will contain the sum of the following forces [25]:

$$\frac{d\vec{r}_i}{dt} = \frac{1}{\gamma} \sum_{j \neq i} \vec{F}_d(\vec{r}_{ij}) + \frac{1}{\gamma} \sum_{j \neq i} \vec{F}_r(r_{ij}) + \vec{F}_B, \quad (3.2)$$

where \vec{r}_i is the position of the i particle, \vec{F}_d is the magnetic force, \vec{F}_r is the repulsive force, and \vec{F}_B is the Brownian force. Moreover $\gamma = 6\pi\eta a$ is the friction coefficient and \vec{r}_{ij} is the vector between the centers of mass of particles i and j . The dipolar force over particle i will be the sum of the dipole-dipole forces exerted by all of the other particles. The dipole-dipole force between particles i and j is given by

$$\vec{F}_d(\vec{r}_{ij}) = \frac{3\mu_0\mu_s m^2}{4\pi r_{ij}^4} \{ [1 - 5(\hat{m} \cdot \hat{r}_{ij})^2] \hat{r}_{ij} + 2(\hat{m} \cdot \hat{r}_{ij}) \hat{m} \}, \quad (3.3)$$

where we take \hat{m} to be aligned always with the field direction. Note that as we are using one-particle Stokes' hydrodynamics, a repulsive force \vec{F}_r must be included to avoid particles from overlapping. This force is calculated from Ref. [43]:

$$\vec{F}_r(r_{ij}) = A \frac{3\mu_0\mu_s m^2}{4\pi(2a)^4} \exp[-B(r_{ij}/(2a) - 1)] \hat{r}_{ij}, \quad (3.4)$$

where we set $A=2$ and $B=10$, so that for two particles that are in mechanical contact the repulsive force exactly balances the attractive dipolar magnetic interaction. Similar repulsive forces have been used in previous works [21,43]. The Brownian force \vec{F}_B is a stochastic force with zero mean, $\langle \vec{F}_B(t) \rangle = 0$, and δ correlated, $\langle F_B(t) F_B(0) \rangle = 2D \delta(t)$, where D is the translational diffusion coefficient $D = k_B T / \gamma$. As usual [1,21,44], we can make the particle evolution equation (3.2) dimensionless, using the particle diameter $2a$ as length scale, so that $r' = r/(2a)$, and a time scale $\tau = 12^2 \eta / (\mu_0 \mu_s M^2)$, such that $t' = t/\tau$. This temporal scale leads to a dimensionless rotational frequency equal to $\Omega \equiv \omega \tau$. This dimensionless frequency is the well-known Mason number with the definition used in Eq. (1.1), $\Omega \equiv \text{Ma}$.

B. Simulation procedure

According to the experimental analysis, we have used only two control parameters, the Mason number Ma and the particle volume fraction ϕ . The simulations being 2D, we

have set the initial average interparticle distance so that it corresponds to the volume fraction in the experiment with the different suspensions.

The numerical integrations have been performed using a time step of 0.005, which has proved to be small enough to avoid significant overlapping errors when the particles come into close contact. We have developed simulations using 400 and 100 particles, and the simulations are carried out in a square box of the proper size to adjust the initial average interparticle distance. Periodic boundary conditions were applied. The particles are set initially at random positions avoiding overlapping, and all of the results reported here are statistical averages over different realizations corresponding to different initial spatial distributions of the particles, typically ten runs. Each simulation is run long enough for the steady state to be reached, and then the quantities to be compared with the experimental results are averaged during the last period of rotation of the field.

The comparison between experimental and simulation results deserves some comments. First, the chains are recognized by means of a criterion according to which two particles are aggregated when the distance between their respective centers of mass is smaller than 1.1 times the particle diameter. Second, using Mie's theory for light scattering by nonspherical objects, we can estimate the scattering dichroism generated from a chain j formed by N_j particles in the forward direction ($\varphi=0$). Actually the scattering dichroism is proportional to the number of particles in the chain, N_j . Assuming that the scattering dichroism produced from a set of chains is the incoherent sum of the scattering dichroism produced by each chain, the total dichroism is proportional to the total number of aggregated particles, N_a . Hence, we will compare the experimental value of the scattering dichroism with the value of N_a obtained in the simulations computed as

$$N_a \equiv \sum_j N_j, \quad (3.5)$$

where the sum is performed for j such that $N_j > 1$. We have computed the dimensionless average chain length (average number of particles in a chain) L in the usual way, i.e., if a chain labeled as j is formed by N_j particles, then

$$L = \frac{\sum_j N_j}{\sum_j 1}. \quad (3.6)$$

The phase lag of a given chain (α_j) is the angular difference between the orientation of the magnetic field and the unit vector parallel to the long axis of the chain. For quasi-linear chains, we have determined the chain orientation vector by calculating the eigenvalues of the chains' inertia tensor, I_j^{\max} , I_j^{\min} . Then, the eigenvector corresponding to I_j^{\min} gives the orientation of the long axis of the chain.

The computations described so far consider straight chains and, obviously, do not take into account the shape of

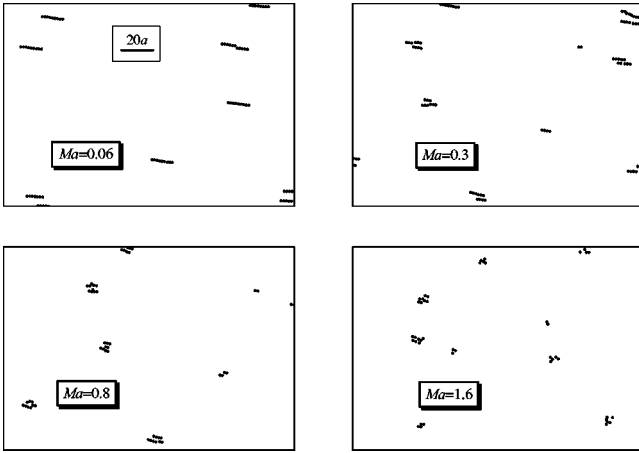


FIG. 6. Particle position in the XY plane at an arbitrary time for different dimensionless rotating frequencies or Mason numbers.

the clusters. However, video microscopy results show that very long chains deviate significantly from straight lines, and, moreover, at high frequencies smaller and more isotropic clusters may appear. To assess the effect of these chain form anomalies in our simulations results, we calculated the same quantities, L and N_a , using a weight function that takes into account the shape of the cluster. Actually we used $W_j = N_j s_j$, where s_j is a shape factor with value 1 for the case of a straight chain, and 0 for a symmetric cluster,

$$s_j = \frac{(I_j^{max})^{1/2} - (I_j^{min})^{1/2}}{(I_j^{max})^{1/2} + (I_j^{min})^{1/2}}. \quad (3.7)$$

We did not observe appreciable changes in the simulation results using this shape correction. Therefore, we present here the results corresponding to the case without the shape factor.

C. Simulation results

1. Very dilute suspension

We have studied the dynamics of very dilute suspensions with the conditions of the microscopy experiments, i.e., volume fraction of particles ($\phi = 10^{-4}$) which corresponds to an initial average separation between particles equal to $R_0/(2a) \sim 16$. The particle diameter is $2a = 1.24 \mu\text{m}$, the magnetization is $M = 2.82 \text{ kA/m}$ (for $H = 1.55 \text{ kA/m}$), and the viscosity of the solvent (water, in this case) at 10°C is $\eta = 1.307 \times 10^{-3} \text{ Pa}\cdot\text{s}$. Using these values we obtain a time scale equal to $\tau = 0.019 \text{ s}$ and $\lambda = 213$. We numerically solved Eq. (3.2) for a system with $N = 400$ magnetic particles. For each dimensionless rotational frequency Ω or Mason number Ma , we calculate the total number of aggregated particles, N_a , and the average length L .

In Fig. 6 we plot the particle positions in the (X, Y) plane for different dimensionless frequencies at an arbitrary time. Several qualitative observations can be made in Fig. 6. First, the size of the structures becomes smaller as the rotational frequency increases. Second, at high Ma , the tendency to form chains aligned with the field is not clearly apparent, and

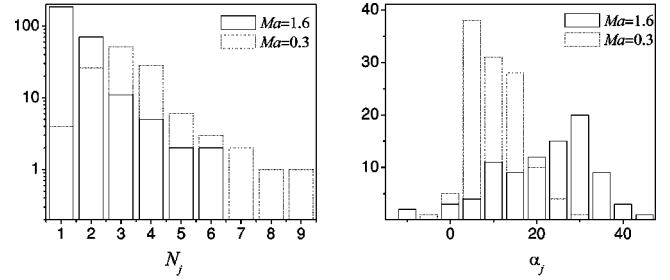


FIG. 7. Distribution of lengths N_j (left) and phase lags α_j (right) at the same arbitrary time of Fig. 6 at a Mason number $Ma = 1.6$ (solid line) and $Ma = 0.3$ (dotted line).

more isotropic clusters appear to be preferred; moreover, a higher number of isolated particles appears. We plot in Fig. 7 the distribution of lengths N_j and phase lags α_j corresponding to the images shown in Fig. 6 at two different Mason numbers. At low Mason numbers $Ma = 0.3$, the distribution of N_j presents a maximum placed around $N_j \sim 3$ while the phase lag follows a narrow distribution around $\alpha_j \sim 5^\circ$. On the other hand, at high Mason numbers $Ma = 1.6$, the maximum of the distribution of N_j is set at $N_j = 1$, which means that there are many isolated particles in the suspension, being responsible to the decrease of the total number of aggregated particles, N_a . At this high Mason number, a broader distribution of α_j appears, and the maximum shifts to higher values.

Some of these observations can be made more quantitative by studying the average chain length. The dimensionless average chain length L versus Ma in a log-log plot is shown in Fig. 8(a). The average chain length follows a power-law behavior with an exponent approximately equal to -0.5 . This behavior agrees well with the one predicted by the chain model developed for ER fluids subject to steady shear flows [38], and for MR suspensions subject to rotating fields [36]. Figure 8(b) shows the total number of aggregated particles, N_a , versus Ma in a log-log plot. Two different regions appear, in agreement with the experimental results. First, there is a plateau zone at low Ma , in which N_a varies very little with Ma . Second, a strongly decreasing response appears for $Ma \geq 1$, with an apparent exponent close to -1 , although the region in which this power-law behavior could be studied in the simulations is rather small.

The picture that emerges from these results is the following: the average chain length decreases monotonously with

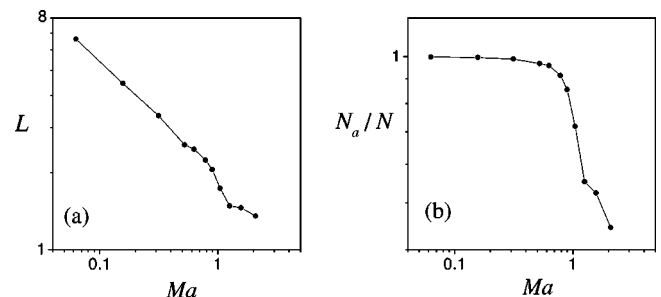


FIG. 8. (a) Average length L and (b) normalized total number of aggregated particles N_a vs Mason number. Suspension with $\phi \sim 10^{-4}$.

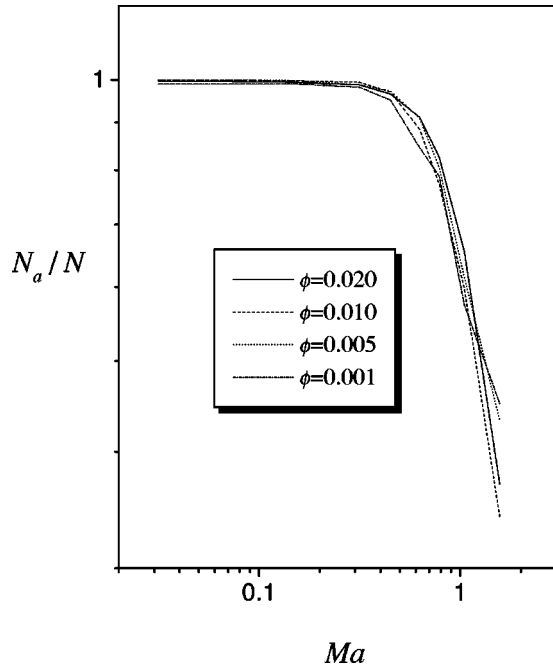


FIG. 9. Normalized total number of aggregated particles vs Mason number at different volume fractions ($0.001 < \phi < 0.02$).

Ma; however, at low Ma, this decrease in length does not show up in the number of aggregated particles, because almost all particles are aggregated although the chains that are stable become shorter as Ma increases. At $Ma_c \sim 1$, the average chain length is approximately 2 [see Fig. 8(a)], which is, obviously, the smallest chain that can be formed. Therefore, at $Ma > 1$, chains formed by two particles become unstable, and, consequently, the total number of aggregated particles starts to decrease.

2. Volume fraction dependence

In this section we described the simulation results which analyze the dynamics of MR suspensions under rotating fields in the conditions of the dichroism experiments, i.e., at different volume fractions, between $\phi = 0.02 - 0.001$. The particle diameter is $2a = 0.9 \mu\text{m}$, the magnetization is $M = 2.72 \text{ kA/m}$, (for $H = 3.1 \text{ kA/m}$) and the viscosity of the solvent (water-glycerol at 50%) at 10°C is $\eta = 9.2 \times 10^{-3} \text{ Pa s}$. Using these values we obtain a time scale equal to $\tau = 0.14 \text{ s}$ and the parameter $\lambda = 75$. We used the initial average separation between particles corresponding to the volume fractions used in the experiments, $R_0/(2a) \sim 4 - 10$. We numerically solved Eq. (3.2) for a system with $N = 100$ particles. In order to compare with the experimental results, for each Mason number, we calculate the total number of aggregated particles, N_a . Figure 9 shows the normalized total number of aggregated particles versus Ma at different volume fractions. It can be clearly seen in this figure how all those curves follow the same behavior. This result confirms that the crossover Mason number does not change with the volume fraction. Therefore, we can conclude that the dynamics of MR suspensions under rotating fields does not show an appreciable change with the volume fraction.

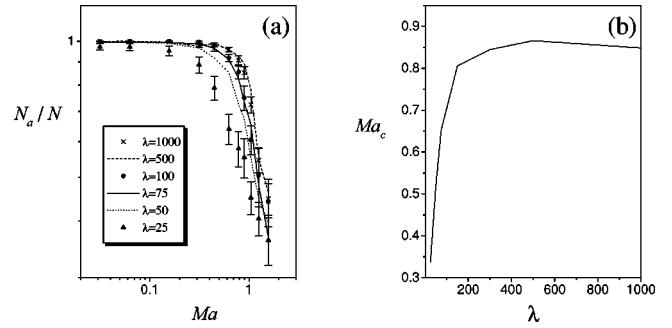


FIG. 10. (left) Normalized total number of aggregated particles, N_a , vs Mason number at different λ : the error bars have only been included for $\lambda = 25, 100, 1000$ (for clarity) (right). Crossover Mason number Ma_c as a function of λ .

3. Thermal effect

In our previous works, we used athermal particle dynamics simulations to interpret similar behaviors. Here, since the average initial distance between particles R_0 is larger than the “thermomagnetic distance” R_1 , we included thermal fluctuations in order to carry out the simulations. However, we have not found any relevant effect in the final state of the system induced by the thermal fluctuations, at least in the analyzed magnitudes; in particular, the number of aggregated particles. In principle, it should be expected that thermal fluctuations might shift the crossover Mason number to a lower value. This hypothesis is reasonable since, roughly speaking, thermal fluctuations avoid the particle aggregation. Then, a lower hydrodynamic force could be required in order to inhibit the aggregation process since, both interactions, the hydrodynamic force and thermal fluctuations, act in the same direction. In order to check this interpretation we have developed simulations at different λ values using a volume fraction of $\phi = 0.02$. We plot in Fig. 10 (left) the normalized total number of aggregated particles versus Ma at different λ values. It can be seen in this figure how at λ values higher than approximately 50 the curves follow the same behavior, that is, the shape and the crossover Mason number remain almost constant. However, for lower λ values the crossover Mason number begins to shift to lower values and the shape of the curves changes. From these curves we calculate the crossover Mason number as each λ value. To compute the Ma_c at each λ we consider the value of the Mason number at which the total number of aggregated particles decreases by 15% from its maximum value. We show in Fig. 10 (right) the Ma_c versus λ . Two different behaviors appear. First, there is a plateau zone at high λ in which Ma_c does not change. In this region the thermal fluctuations could be neglected in order to interpret the dynamics of MR suspensions under rotating fields. Second, a strongly decreasing dependence appears for $\lambda < 50$. These results indicate that for low values of λ (approximately 50), thermal fluctuations become relevant in the dynamics of MR suspensions under rotating fields.

IV. CONCLUSIONS

The purpose of this work was to study the spatiotemporal evolution of the induced structures in very dilute polarizable

colloidal suspensions subject to rotating magnetic fields by means of video microscopy experiments. This technique us allows us to directly visualize the dynamics and needs of very dilute suspensions ($\phi \sim 10^{-4}$). The average chain length decreases when increasing frequency. We also found that there is a crossover Mason number above which the rotation of the field prevents the particle aggregation to form chains. Therefore, at these high Mason numbers, more isotropic clusters and isolated particles appear. The same behavior was also found in previous scattering dichroism experiments on more concentrated suspensions.

In order to study the role played by the volume fraction, we carried out scattering dichroism experiments in suspensions with low concentration ($\phi \sim 0.001-0.02$). Dichroism shows two distinct regions, above and below Ma_c . The crossover Mason number does not depend on the volume fraction which points out the generality of this behavior. We can conclude that the results obtained here (the Mason num-

ber governs the dynamics of chain rotation, the limits to the rotational dynamics come from both the mechanical instability of the chains due to shear and the formation of more isotropic structures) can be extrapolated to higher volume fractions, provided they are below a threshold volume fraction above which sheetlike structures will form [21].

Thermal particle dynamics simulations are also reported, showing good agreement with the experiments. We theoretically analyzed the thermal effect on the dynamics observing a decrease of the crossover Mason number for $\lambda < 50$.

ACKNOWLEDGMENTS

This research was partially supported by the DGICYT Project No. BFM2000-0019. We gratefully acknowledge T. Madrid for developing software to improve image quality and to calculate the Hough transform. We also thank James E. Martin for fruitful discussions.

-
- [1] R.G. Larson, *The Structure and Rheology of Complex Fluids* (Oxford University Press, New York, 1999), Chap. 8.
 - [2] J. Carlson, D. Catanzarite, and K.S. Clair, *Int. J. Mod. Phys. B* **10**, 2857 (1996).
 - [3] *Proceedings of the Eighth International Conference on Electrorheological Fluids and Magnetorheological Suspensions*, edited by G. Bossis (World Scientific, Singapore, 2002), pp. 1–328.
 - [4] A.S. Lübbe, C. Bergemann, J. Brock, and D.G. McClure, *J. Magn. Magn. Mater.* **194**, 149 (1999).
 - [5] J. Liu, G.A. Flores, and R. Sheng, *J. Magn. Magn. Mater.* **225**, 209 (2001).
 - [6] G. Bossis and E. Lemaire, *J. Rheol.* **35**, 1345 (1991).
 - [7] E.M. Furst and A.P. Gast, *Phys. Rev. E* **61**, 6732 (2000); **62**, 6916 (2000).
 - [8] E. Lemaire, Y. Grasselli, and G. Bossis, *J. Phys. II* **2**, 359 (1992).
 - [9] M. Fermigier and A.P. Gast, *J. Colloid Interface Sci.* **154**, 522 (1992).
 - [10] Y.H. Hwang and X.I. Wu, *Phys. Rev. E* **49**, 3102 (1994).
 - [11] D. Wirtz and M. Fermigier, *Phys. Rev. Lett.* **72**, 2294 (1994).
 - [12] J.H.E. Promislow, A.P. Gast, and M. Fermigier, *J. Chem. Phys.* **102**, 5492 (1995).
 - [13] S. Melle, M.A. Rubio, and G.G. Fuller, *Phys. Rev. Lett.* **87**, 115501 (2001).
 - [14] G. Helgesen, P. Pieranski, and A.T. Skjeltorp, *Phys. Rev. Lett.* **64**, 1425 (1990).
 - [15] G. Helgesen, P. Pieranski, and A.T. Skjeltorp, *Phys. Rev. A* **42**, 7271 (1990).
 - [16] J.C. Bacri, A. Cebers, and R. Perzynski, *Phys. Rev. Lett.* **72**, 2705 (1994).
 - [17] B.E. Kashevsky and A.L. Novikova, *Magnetohydrodynamics* (N.Y.) **25**, 304 (1989).
 - [18] P. Meakin and A.T. Skjeltorp, *Adv. Phys.* **42**, 1 (1993).
 - [19] B.E. Kashevsky, *J. Magn. Magn. Mater.* **122**, 34 (1993).
 - [20] M. Fermigier and A.P. Gast, *J. Magn. Magn. Mater.* **122**, 46 (1993).
 - [21] J.E. Martin, R.A. Anderson, and C.P. Tigges, *J. Chem. Phys.* **108**, 7887 (1998).
 - [22] O. Volkova, S. Cutillas, P. Carletto, G. Bossis, A. Cebers, and A. Meunier, *J. Magn. Magn. Mater.* **201**, 66 (1999).
 - [23] G. Bossis and A. Cebers, *J. Magn. Magn. Mater.* **201**, 218 (1999).
 - [24] J.E. Martin, *Phys. Rev. E* **63**, 011406 (2001).
 - [25] J.E. Martin, R.A. Anderson, and C.P. Tigges, *J. Chem. Phys.* **110**, 4854 (1999).
 - [26] S. Melle, G.G. Fuller, and M.A. Rubio, *Phys. Rev. E* **61**, 4111 (2000).
 - [27] S. Melle, O.G. Calderón, G.G. Fuller, and M.A. Rubio, *J. Colloid Interface Sci.* **247**, 200 (2002).
 - [28] H.C. van de Hulst, *Light Scattering by Small Particles* (Dover, New York, 1981).
 - [29] O. Sandre, J. Browaeys, R. Perzynski, J.C. Bacri, V. Cabuil, and R.E. Rosensweig, *Phys. Rev. E* **59**, 1736 (1999).
 - [30] A.P. Gast and C.F. Zukoski, *Adv. Colloid Interface Sci.* **30**, 153 (1989); Mason number was first introduced in literature for ER fluids under steady shear.
 - [31] O. Volkova, S. Cutillas, and G. Bossis, *Phys. Rev. Lett.* **82**, 233 (1999).
 - [32] J.F. Canny, *IEEE Trans. Pattern Anal. Mach. Intell.* **8**, 679 (1986).
 - [33] R.C. Gonzalez and R.E. Woods, *Digital Image Processing* (Addison Wesley, Reading, MA, 1992), Chap. 7.
 - [34] G.G. Fuller, *Optical Rheometry in Complex Fluids* (Oxford University Press, Oxford, 1995).
 - [35] S. Melle, O.G. Calderón, G.G. Fuller, and M.A. Rubio, *J. Non-Newtonian Fluid Mech.* **102**, 135 (2002).
 - [36] S. Melle and J.E. Martin, *J. Chem. Phys.* **118**, 9875 (2003).
 - [37] J.E. Martin, E. Venturini, J. Odinek, and R.A. Anderson, *Phys. Rev. E* **61**, 2818 (2000).
 - [38] J.E. Martin and R.A. Anderson, *J. Chem. Phys.* **104**, 4814 (1996).
 - [39] T.C. Halsey, R.A. Anderson, and J.E. Martin, *Int. J. Mod. Phys. B* **10**, 3019 (1996).

- [40] M. Whittle, *J. Non-Newtonian Fluid Mech.* **37**, 223 (1990).
- [41] J.R. Melrose and D.M. Heyes, *J. Chem. Phys.* **98**, 5873 (1993).
- [42] M. Mohebi, N. Jamasbi, G.A. Flores, and J. Liu, *Int. J. Mod. Phys. B* **13**, 2060 (1999).
- [43] M. Mohebi, N. Jamasbi, and J. Liu, *Phys. Rev. E* **54**, 5407 (1996).
- [44] D.J. Klingenberg, F. van Swol, and C.F. Zukovski, *J. Chem. Phys.* **91**, 7888 (1989).